Stability of binary colloidal crystals immersed in a cholesteric liquid crystal

Setarehalsadat Changizrezaei[*]

Department of Applied Mathematics, The University of Western Ontario, London, Ontario N6A 5B8, Canada

Colin Denniston[†]

Department of Applied Mathematics, The University of Western Ontario, London, Ontario N6A 5B8, Canada
and Department of Physics and Astronomy, The University of Western Ontario, London, Ontario N6A 5B8, Canada

In this paper, we model a number of both closed-packed and non-closed-packed crystals inside a cholesteric liquid crystal (LC) with different pitch values and nematic LC through the Landau–de Gennes free-energy method. We used binary boundary conditions (normal and planar anchoring) applied on the surface of colloids as we are interested in investigating the stability of binary crystals. The results indicate that body-centered-cubic (BCC) crystals have a lower-energy lattice defect structure than the diamond crystal, and the most energetically favorable BCC lattice can be formed in a cholesteric liquid crystal with a pitch value commensurate with the lattice spacing. Furthermore, it is shown that a pair of binary colloids can be self-assemble into a stable face-centered-cubic lattice structure inside a nematic LC, as it has the lowest energy comparing to diamond and BCC crystals.

I. INTRODUCTION

Liquid crystals (LC) are widely used in a variety of applications [1–3]. One potential application is as a photonic material when combined with a self-assembled colloidal crystal inside the LC. Photonic crystals are formed from a periodic organization of particles, of size comparable to the wavelength of light, which represents a periodic dielectric pattern in space. Colloidal crystals are composed of a periodic lattice of colloids within a macroscopic media resulting a periodic dielectric function. As a result, they can be used as the basis of photonic crystals. Therefore, self-assembly of colloidal particles in a fluid has been studied as a potentially efficient method to generate photonic crystals [4–6]. The resulting phonotic band structures can be used to control and confine electromagnetic waves due to refraction and reflection of light from different interfaces in the periodic dielectric medium. This behavior is similar to electron propagation in semiconductors [7]. For this purpose, the presense of a photonic band gap is desirable, meaning there is a certain range of frequencies for electromagnetic waves that is forbidden to be propagated in all directions of wave propagation [8]. Closed-packed crystals' photonic band structure typically do not possess photonic band gaps, but in 1990 it was found that a diamond structure of spheres in empty space does show a complete band gap [9]. This makes it particularly interesting to investigate colloidal crystal structures that are stable in a non-closed-packed configuration.

Self-assembly of particles inside a LC provides a method to generate colloidal photonic crystals [4–6,10]. A simple fluid is not an ideal medium to produce a non-closed-packed structure as most colloidal interactions are isotropic and spherically symmetric (which typically leads to close-packed crystal structures). However, a potentially ideal host medium for generating non-closed-packed structures is a liquid crystal. As LCs have anisotropic properties, long-range anisotropic interactions exist between the colloidal particles. When particles are immersed in LCs, the LC molecules are distorted around the particles from their preferred uniform orientation due to the imposed boundary conditions on the particle's surface. The distortions often produce topological defects, and the director distortion increases the elastic free energy of the system [11,12]. The long-range anisotropic forces are induced between the particles as sharing the distortion volumes around the particles helps minimize the elastic free energy [13–17]. The imposed boundary conditions on the surface of the particles dictates the type of topological defects and the induced interactions.

In a nematic, when the preferred orientation of LC molecules on the surface of colloids is parallel (planar anchoring), a pair of defects are generated at the poles of particles, called boojums [11]. The boojum cores can be single, split, and double cores [18]. The stable single core can be found at weak anchoring, small particles, and high temperature. The split cores are a pair of $+1/2$ point defects connected by a defect line of the same strength. If the defect line connecting a pair of split core boojums is not developed completely, then the defect structure is known as a double boojum. In contrast, when there is normal anchoring of LC molecules on the surface of colloids, two possible defect structures can be generated in nematic LC. One possible defect is a Saturn ring defect, which is a disclination defect line surrounding around the particle inducing a long-range quadropolar interaction and

*schangiz@uwo.ca
†cdennist@uwo.ca

stable for small particles, and another possibility is a -1 point defect, called a hyperbolic hedgehog, inducing far-field dipolar interaction [11,12,19–22].

When the colloids are immersed inside a cholesteric LC, the associated defect lines become twisted around them. Depending on the size of the pitch in cholesteric LC and size of colloid, a broad range of defect structures can be seen [14]. Considering colloids with strong planar anchoring inside a cholesteric LC, a defect-bonded chain is generated by connecting the boojum handles from adjacent particles [17]. Moreover, a blue phase LC can produce a three-dimensional (3D) disclination network. As a result, colloidal-blue phase composites can be generated as the colloids are attracted to the 3D defect network depending on the anchoring strength [23,24]. Also, the stability of a diamond colloidal crystal with normal anchoring inside a cholesteric LC through its phonon spectrum is investigated in Ref. [25]. In this 3D self-assembled structure, the defect lines travel along the symmetry axes of the diamond crystal.

Binary particles with normal and planar anchoring inside a nematic LC can self-assemble into 2D crystals, such as a 2D square crystal [26,27]. The anisotropic interactions between colloids with heterogeneous boundary conditions inside both nematic and cholesteric LC are studied in Ref. [27]. In this paper, it was found that multiple local minima exist in 3D space when binary colloids are placed inside cholesteric LC with different pitch values and there are short-range attractive forces induced between colloids. So we can conclude that a variety of potential crystals including closed-packed and non-closed-packed structures could potentially be formed inside cholesteric LC using these binary particles as the basis for the lattice.

In this paper, we examine binary colloidal crystal structures, and in particular diamond and BCC lattices, inside a cholesteric LC. We test different helical pitch values commensurate with our system size in order to measure the binary advantage energy for each of the colloidal crystals, find the pitch value at which the most energetically favorable defect structure occurs, and then compare the stability of closed-packed and non-closed-packed crystals. We also investigate the defect structure of diamond, BCC, and FCC lattices inside a nematic LC to find the potential stable crystal.

II. MODELLING

Using the Landau–de Gennes formalism [28], the LC is modeled by a tensor order parameter Q to describe the LC molecules orientation. This tensor is defined as $Q_{ij} = \langle \hat{m}_i \hat{m}_j - \frac{1}{3}\delta_{ij} \rangle$, which is the ensemble average of the individual molecular orientation $\hat{m}$. **Q** is a symmetric traceless matrix. Its largest eigenvalue is $\frac{2}{3}q$ ($0 < q < 1$) and represents the magnitude of order along the corresponding eigenvector $\hat{\mathbf{n}}$, which defines the director field. The evolution of Q can be tracked using Beris and Edwards theory [29] as follows:

$$(\partial_t + \boldsymbol{u} \cdot \nabla)\boldsymbol{Q} - \boldsymbol{S}(\boldsymbol{W}, \boldsymbol{Q}) = \Gamma \boldsymbol{H}, \tag{1}$$

where $\boldsymbol{H}$ is the molecular field, $\boldsymbol{u}$ is the fluid velocity, and Γ is a rotational diffusion constant. Also $\boldsymbol{S}(\boldsymbol{W}, \boldsymbol{Q})$ is related to the symmetric and antisymmetric component of velocity

gradient as:

$$\boldsymbol{S}(\boldsymbol{W}, \boldsymbol{Q}) = (\xi \boldsymbol{D} + \Omega)(\boldsymbol{Q} + \boldsymbol{I}/3) + (\boldsymbol{Q} + \boldsymbol{I}/3)(\xi \boldsymbol{D} - \boldsymbol{\Omega})$$
$$- 2\xi(\boldsymbol{Q} + \boldsymbol{I}/3)\mathrm{Tr}(\boldsymbol{Q}\boldsymbol{W}), \tag{2}$$

where the symmetric and antisymmetric velocity gradient components, $\boldsymbol{D} = (\boldsymbol{W} + \boldsymbol{W}^T)/2$ and $\boldsymbol{\Omega} = (\boldsymbol{W} - \boldsymbol{W}^T)/2$, are related to $W_{\alpha\beta} = \partial_\beta u_\alpha$. ξ is related to the effective aspect ratio of LC molecule.

The right-hand side of Eq. (1) drives the system toward a free-energy minimum through the functional derivative of the free energy:

$$\boldsymbol{H} = -\frac{\delta F}{\delta Q} + \left(\frac{\boldsymbol{I}}{3}\right)\frac{\delta F}{\delta Q}. \tag{3}$$

In our work, the whole free energy of the system is composed of the bulk free energy and elastic and surface energies:

$$F = \int \{F_{\text{bulk}} + F_{\text{elastic}}\}dV + \int F_{\text{surface}}\, dS. \tag{4}$$

The bulk free energy of the system is described as:

$$F_{\text{bulk}} = \frac{A_0}{2}\left(1 - \frac{\gamma}{3}\right)Q_{\alpha\beta}^2 - \frac{A_0\gamma}{3}Q_{\alpha\beta}Q_{\beta\gamma}Q_{\gamma\alpha}$$
$$+ \frac{A_0\gamma}{4}\left(Q_{\alpha\beta}^2\right)^2, \tag{5}$$

where A_0 is a constant, and the phase transition between isotropic and LC phases can be controlled through γ. In order to have a stable LC phase, γ is set to 3.2 (the isotropic fluid is stable when $\gamma < 2.7$, the LC is stable when $\gamma > 3.0$, and coexistence is possible for $2.7 < \gamma < 3.0$).

F_{elastic} represents the elastic distortion via

$$F_{\text{elastic}} = \frac{L_1}{2}(\partial_\alpha Q_{\beta\gamma})^2$$
$$+ \frac{L_2}{2}(\partial_\alpha Q_{\alpha\gamma})(\partial_\beta Q_{\beta\gamma})\frac{4\pi L_1}{P}\epsilon_{\alpha\beta\gamma}Q_{\alpha\nu}(\partial_\beta Q_{\gamma\nu}). \tag{6}$$

The usual distortions in a nematic LC are represented through the first two terms. The last term is present to model a cholesteric LC with a helical twist pitch P in the director which minimizes this term. L_1 and L_2 are the elastic constants, which can be mapped to the Frank elastic constants K_1, K_2, K_3 [29]. In our work, we chose $K_1 = K_3$ and $K_2 < K_1$ and K_3 to have a stable cholesteric LC. However, in nematic LC, we chose $K_1 = K_2 = K_3$.

Finally, F_{surface} is associated with the interaction of LC molecules with the surface of the colloidal particles. In our work, the preferred orientation of LC molecules on the surface of the colloids is either normal or planar anchoring. Anchoring strength is controlled through a parameter α_s. We use a large-enough value of α_s to have strong anchoring. The imposed planar and normal LC molecule anchoring on the colloid surface is induced by:

$$F_{\text{surface}} = \frac{\alpha_s}{2}\left(Q_{ij} - Q_{ij}^0\right)^2 \rightarrow \text{Normal anchoring}, \tag{7}$$

$$F_{\text{surface}} = \frac{\alpha_s}{2}\left(\tilde{Q}_{ij} - \tilde{Q}_{ij}^{\perp}\right)^2 \rightarrow \text{Planar anchoring}, \tag{8}$$

TABLE I. Simulation parameters.

Symbol	Value	Units
A_0	0.5	atm
γ	3.103	—
K_1	15	pN
K_2	6.7,15	pN
K_3	15	pN
Γ	0.33775	atm^{-1} μm^{-1}
ξ	0.52	—
Δx	0.0625	μm
Δt	0.5	μs
P_0	1.0	atm

where $Q_{ij}^0 = q^0(\hat{n}_i{}^0 \hat{n}_j{}^0 - \frac{1}{3}\delta_{ij})$, $\hat{n}^0$ is the normal to the surface of particle, and q^0 is the equilibrium bulk value of q. Also, $\tilde{Q}_{ij} = Q_{ij} + \frac{1}{3}q^0\delta_{ij}$ and $\tilde{Q}_{ij}^{\perp} = (\delta_{ik} - \hat{n}_i{}^0 \hat{n}_k{}^0)\tilde{Q}_{kl}(\delta_{lj} - \hat{n}_l{}^0 \hat{n}_j{}^0)$ is the projection of $\tilde{Q}_{ij}$ onto the tangent plane of the surface [30].

The LC also satisfies the Navier-Stokes and continuity equations with the following symmetric:

$$\sigma_{\alpha\beta} = -P_0\delta_{\alpha\beta} - \xi H_{\alpha\gamma}\left(Q_{\gamma\beta} + \frac{1}{3}\delta_{\alpha\beta}\right)$$

$$- \xi\left(Q_{\alpha\gamma} + \frac{1}{3}\delta_{\alpha\gamma}\right)H_{\alpha\beta}$$

$$+ 2\xi\left(Q_{\alpha\beta} + \frac{1}{3}\delta_{\alpha\beta}\right)Q_{\gamma\epsilon}H_{\gamma\epsilon}$$

$$- \partial_\beta Q_{\gamma\nu}\left(\frac{\delta F}{\delta \partial_\alpha Q_{\gamma\nu}}\right) \qquad (9)$$

and antisymmetric tensors:

$$\tau_{\alpha\beta} = Q_{\alpha\gamma}H_{\gamma\beta} - H_{\alpha\gamma}Q_{\alpha\beta}. \qquad (10)$$

These equations are solved using a lattice Boltzmann algorithm described in Refs. [31–34].

Using the above equations, the corresponding stresses and forces can be calculated in the fluid and then applied to the colloids. The fluid-colloid interaction is modeled by mapping the colloids onto the fluid mesh on which the lattice Boltzmann method is defined. In this method, each spherical colloid is first discretized into 6252 nodes, and then the nodes are coupled to the fluid mesh through interpolating onto nearby fluid lattice sites. The details of this method are described in Refs. [13,35–39]. The algorithm was performed using a custom LAMMPS [40] package. The simulation parameters used are given in Table I.

The full three-dimensional computation of the liquid crystal and colloid dynamics is quite costly and so we break it into stages in order to minimize this cost. We first examine the energy of several candidate crystal states of colloids inside the LC. As such, the dynamics in this case are just used to take us to a minimum of the liquid crystal energy given the fixed colloid configuration. We then applied LC forces onto the particles to measure the phonon frequencies of the lowest energy lattice found and establish its stability when allowing the colloids positions to fluctuate.

III. RESULTS

In nature there are several stable binary atomic crystal structures such as SiC, ZnC, etc. We examine several of these lattice structures as potential candidates for our colloidal crystal. The binary colloids will be formed from spherical particles with two different boundary conditions for the director (normal and planar) on the surface of the sphere. Once immersed in the LC, the particles induce defects in the LC matrix and these defect dominate the interactions of the particles. We investigated similar heterogeneous particle pairs inside a LC in Ref. [27]. Once placed in a crystal lattice the defect structure can be quite different from that found for a single pair. How the defects align with the lattice also affects the overall stability of the crystal [25].

In the first subsection, the defect structures of a body-centered-cubic (BCC) and diamond lattice with binary basis particles inside a cholesteric LC with different pitch values are investigated. We examine which lattice has the lowest energy per particle and hence could be as a potential stable crystal for binary particles in cholesteric LC. In the second subsection, we did the same simulations for face-centered-cubic (FCC), BCC, and diamond lattices inside a nematic LC. Commensurability issues mean that a FCC and BCC are unlikely to be competing lattice structures at a fixed cholesteric pitch, so we only compare the FCC for the nematic case.

A. Cholesteric LC

1. Diamond lattice

We first considered a colloidal crystal in a diamond lattice with a unit cell composed of eight particles of radius 1.06 μm ($17\Delta x$) inside a cholesteric LC. The simulation box dimensions are ($L \times L \times L$) with $L = 5.5$ μm, or ($88 \times 88 \times 88$)Δx, and is periodic in the x, y, and z directions. In this case, the nearest surface to surface separation is about $4\Delta x$. Similarly to Ref. [25], the closest nearest surface separation is chosen in a way that it is large enough so the particle surfaces do not overlap each other and small enough so that the director distortion of one particle can affect its neighboring particles.

The colloidal particles have binary boundary conditions (normal and planar) on the particle surfaces. As shown in Fig. 1, the binary diamond lattice consists of two FCC lattices displaced from each other by ($\frac{a}{4}$, $\frac{a}{4}$, $\frac{a}{4}$), where a is the lattice constant of the cubic super cell. The colloids from the two different FCC lattices are shown in different colors. The director field is aligned perpendicularly on the surface of particles in blue (dark) and tangentially on the green (lighter) particles.

The lattice structure is immersed in a cholesteric LC. Several values of the pitch are investigated in order to examine the resulting LC configuration that is obtained by running the equations of motion toward their steady state. To compare various crystal structures we will examine the particle energy for the configuration:

$$\Delta E/n = (E_n - E_0)/n. \qquad (11)$$

This measures the increase of free energy per particle when n particles ($n = 8$ for a diamond unit cell, $n = 2$ for a BCC unit cell, and $n = 4$ for a FCC unit cell using a standard cubic unit
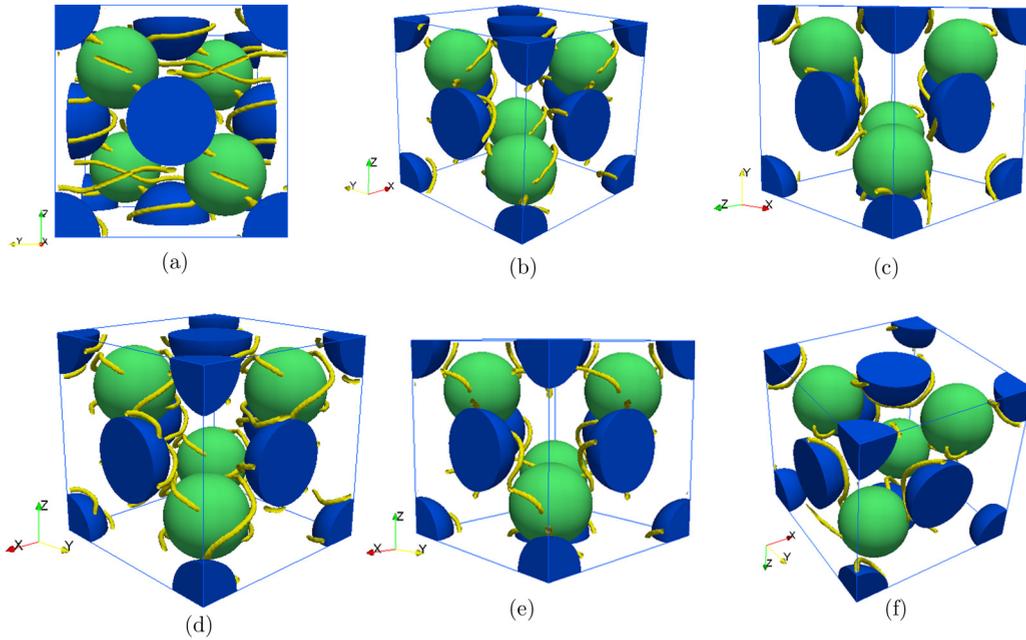
FIG. 1. Unit cell of binary diamond colloidal crystal in cholesterics with different pitches. There is planar anchoring on the surface of green colloids and normal anchoring on the surface of blue colloids. There are eight particles inside the unit cell. The defect structures (disclinations) are shown in yellow. The pitch values are (a) and (d) (first column) $L/2 = 44\Delta x$, (b) and (e) (second column) $L = 88\Delta x$, and (c) and (f) (third column) $2L = 176\Delta x$, where L is the size of a unit cell. The top row shows the configuration with the lowest energy found for a given pitch, whereas the bottom row shows the highest energy configuration found for a given pitch.

cell) are placed in the crystal configuration as compared to the same system size with no particles (E_0). It is reasonable to assume that the director field must have the same periodicity as the crystal in order for the lattice to be stable. As such, the director field must be aligned at the systems (periodic) boundaries. In a cholesteric LC this means it can only rotate by multiples of π in the direction of a twist axis. As a result, we cannot choose arbitrary pitch values as they should be commensurate with the size of the lattice constant. Therefore, we used three different pitch values λ where the director twists over the distance L by 2π ($\lambda = 88\Delta x = L$), 4π ($\lambda = 44\Delta x = L/2$), and π ($\lambda = 176\Delta x = 2L$).

First, we examine a diamond colloidal crystal placed inside a cholesteric LC with a pitch value of $88\Delta x$ (director twists by 2π over box size L). The twist axis in the cholesteric LC is initially along the z direction. We performed several simulations initialized with different initial values for the angle between the director and x axis. Ideally, the final state would be independent of the initial conditions. Unfortunately, the system easily gets stuck in localized states. While in many cases the states only differ slightly in energy (see Fig. 2), there are cases where different defect structures can be found depending on the initial θ values. The extreme cases are shown in Figs. 1(b) and 1(e). While the defect lines look similar in the two cases, the lower-energy case [Fig. 1(b)] has slightly shorter defect lines which are localized to a single colloid. We will return to the question of whether we have found the global minimum later when we look at the stability of these structures.

Next, the diamond colloidal crystal was inserted inside a cholesteric LC with smaller pitch value of $44\Delta x$ (director twists by 4π over box size L). Again, depending on the initial

angle we set the director, we arrive at different local minima. As it can be seen in the Fig. 2, the lowest-energy crystal can be found at $\theta = 3°$, and its corresponding defect configuration is shown in Fig. 1(a). In this case, the defect lines stretch across the lattice in order to reduce distortion in the LC medium, but these lines tend to flow more along the x and y directions rather than z, suggesting a memory of the initial orientation of the pitch. It is worth mentioning that small pitch value makes the defect lines more twisted around the colloid [41]. The higher-energy local minima found are typically more disordered in their disclination structure, as seen in Fig. 2(d). Finally, we investigated the defect structure of the diamond lattice inside a cholesteric LC with the larger pitch value of $176\Delta x$ (director twists by 2π over box size L). The defect configurations are shown in Figs. 1(c) and 1(f) and are quite
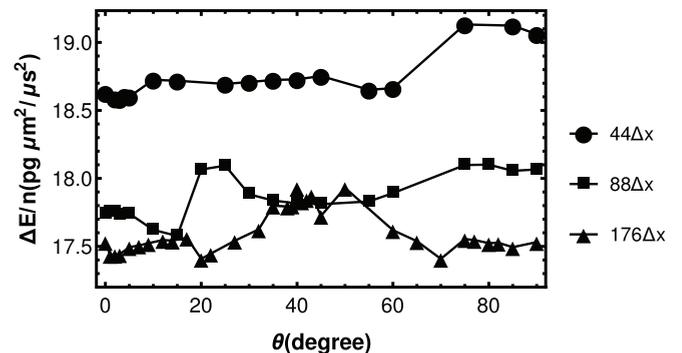
FIG. 2. The energy gained per particle for binary diamond colloidal crystal ($n = 8$) inside a choelsteric LC with pitch values of $88\Delta x$, $44\Delta x$, and $176\Delta x$ as a function of θ.

localized to each colloid. Again, the energy landscape of the local minima is quite jagged, as shown in Fig. 1.

In summary, for all cases examined of the diamond colloidal lattice, the energy landscape is quite rough and the defect lines do not really respect the symmetries of the lattice. As we shall see later, none of these structures are good candidates for the true energy minima of this system.

2. BCC lattice

Next, we examine the energy of particles with binary boundary conditions as a basis for a binary BCC lattice. We chose a BCC instead of, say, an FCC lattice, as it is possible to have a BCC lattice with the same particle sizes and separations and unit cell size as the diamond lattice. As such, we can directly compare the energies of the two crystals at the same pitch (again, chosen commensurate with the unit cell), as it is possible for the system to go from one configuration to the other. With the same nearest-neighbor particle as we used in diamond lattice, we can actually construct a smaller BCC unit cell with size $(44 \times 44 \times 44)\Delta x$. In this case, the pitch values used for the diamond simulations are still commensurate with the system size, except for the larger one (where the director twists by π over a distance $L = 88\Delta x$), where we will need to use a $2 \times 2 \times 2$ unit cell system in order to have commensurability.

Similarly to the diamond simulations, we measured the energy per particle using Eq. (11) ($n = 2$ particles per BCC unit cell). We first considered the BCC unit cell in a cholesteric LC with pitch value of $88\Delta x$, and the lowest energy defect patterns can be seen in Fig. 3(a). The central green colloid has planar anchoring and the blue ones at the corners have normal anchoring. The plot of the energy per particle is shown in Fig. 4 as a function of an initialization angle for the director. The energy landscape for the BCC crystal is much more regular and symmetric than found for the diamond crystal and almost identical defect structures are found for many different initial configurations. The minimum in energy occurs at $\theta = 45°$, and the defect lines are twisted in a way producing less distorted volume in the unit cell and they travel along the symmetry axes of the BCC unit cell. The higher energy configurations typically have a slightly longer defect lines somewhere in the system, potentially in pairs that cannot easily be relaxed.

Next, similar simulations are performed for BCC unit cell in LC with a higher pitch value $176\Delta x$. In this case, we considered a system considered of $2 \times 2 \times 2$ unit cells in each direction so that the director field rotates by π in the box of size $(88 \times 88 \times 88)\Delta x$. Considering the Fig. 4, the energy curve is smooth and almost the same defect configuration is found for most cases. A minimum in energy again is found for initial $\theta = 45°$, corresponding to the defect structures presented in Fig. 3(c). As can be seen in this figure, the defect lines are symmetrically joined between the spheres, leading to the lower energy in the system (the green colloids have planar anchoring and the blue ones have normal anchoring).

Finally, the BCC crystal is examined in a cholesteric LC with the lower pitch value of $44\Delta x$. The plot of energy in Fig. 4 shows that the lowest energy BCC colloidal crystal can be found at both $\theta = 5°$ and $\theta = 80°$, producing the lowest

(a)

(b)

(c)
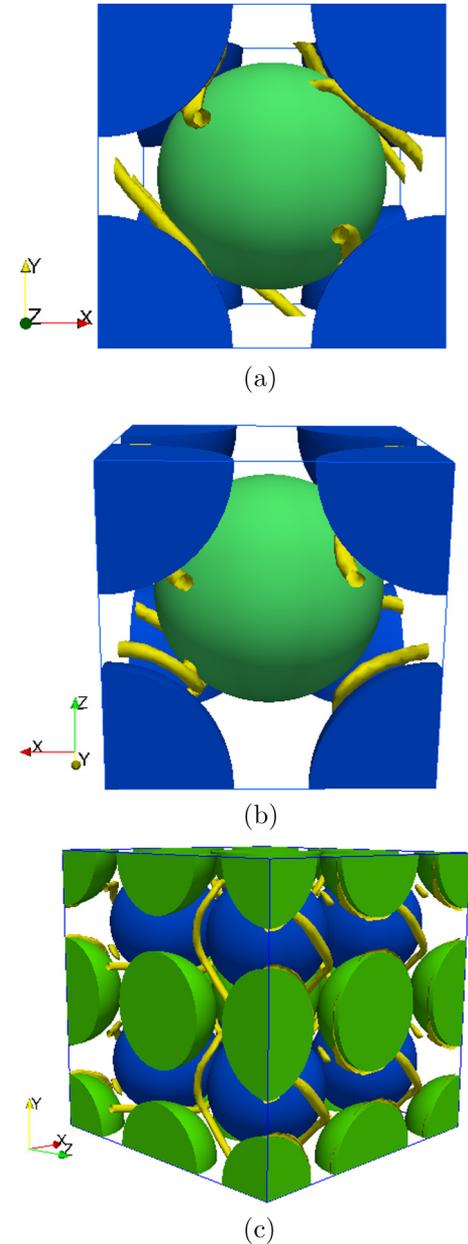
FIG. 3. The defect structures for a BCC colloidal crystal inside a cholesteric LC with different pitch values (a) $88\Delta x$ with $\theta = 45°$, (b) $44\Delta x$ with $\theta = 5°$, and (c) $176\Delta x$ with $\theta = 2°$.

distorted volume in the BCC unit cell. The same sorts of defect structure exist for both angles, but the lines are twisted in opposite directions [Fig. 3(b)]. All defect configurations at $25° < \theta < 60°$ are in the same higher-energy state corresponding to the most distorted unit cell.

Overall, we see the energy landscape for the BCC lattice being more symmetric and not as rugged as found for the diamond lattice. In addition, the defect lines that form in the lowest energy states found for the BCC lattice tend to follow lines of symmetry in the lattice for the shorter pitches. For the longest pitch, there are noticeably more defect lines [cf. Fig. 3(c)] in the system. We also note that with the exception of the longest pitch, the energies for the BCC lattice are lower than those found for the diamond lattice.
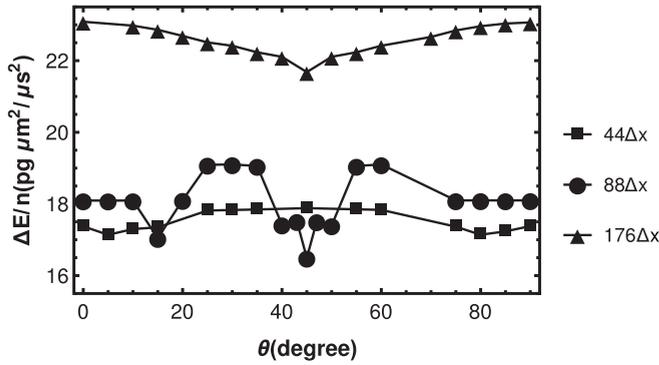
FIG. 4. The energy gained per particle for binary BCC colloidal crystal ($n = 2$ per unit cell) inside a choelsteric LC with pitch value of $88\Delta x$, $44\Delta x$, and $176\Delta x$ as a function of θ. The energy for BCC in cholesteric LC with highest pitch value is divided by 16 as there are totally eight unit cells in our system.

B. Nematic LC

It is also interesting to examine these lattice structures in a nematic (corresponding to a cholesteric with infinite pitch). In this case, there is evidence from experiments [26] that one can arrange the binary particles into a 2D square lattice with alternating particle types, similarly to the structure show schematically in Fig. 5. There are multiple ways to generalize this into a 3D lattice. Given that the particles were quite closely packed in the experiment, the most natural generalization is to take the 2D structure as a face of a FCC lattice. In order to have the same closest surface to surface separation of $4\Delta x$, a FCC unit cell of size $(54 \times 54 \times 54)\Delta x$ is considered. The plot of energy and defect structures are shown in Figs. 6 and 7. In this case, almost all initial orientations of the director end up in essentially the same state. The lowest-energy defect structure is shown in Fig. 7(c).

For comparison to the lattices examined in the cholesteric we will also examine a BCC and a diamond lattice in a nematic. For both cases the states found are again nearly independent of the initial orientation, except for a few cases,
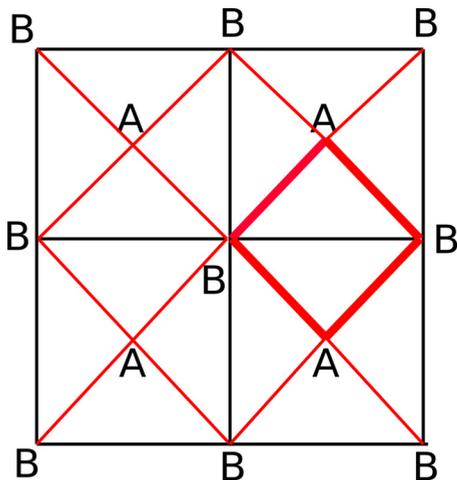
FIG. 5. Face of FCC lattice gives a square lattice in 2D.
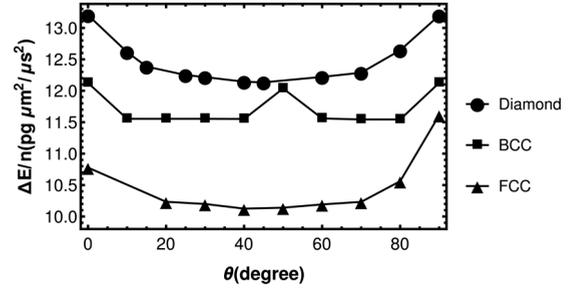
FIG. 6. The energy gained per particle for binary BCC ($n = 2$), FCC ($n = 4$), and diamond ($n = 8$) colloidal crystal inside a nematic LC as a function of θ.

as seen in Fig. 6. The corresponding minimal energy states are shown in Fig. 7.

C. Stability

Comparing the energies for both BCC and diamond crystals in a cholesteric LC, it can be concluded that the most energetically favorable crystal is BCC, as it has lower energy defect structure with more symmetric defect lines in LC with pitch value of $88\Delta x$. However, by itself this does not mean that it would not be possible to produce a diamond crystal with some metastability as energy barriers between states could quite easily be larger than thermal energies ($k_B T$). To test the stability of the crystal structures found so far, we add thermal noise to the molecular field **H** in the liquid crystal and allow the particles to move in response. These simulations are much more costly than just finding the minima so we will restrict ourselves to looking at the most promising cases found so far.

For the diamond lattice in the cholesteric the lowest energy state found was for the longest pitch. However, once we allow the particles to move in response to thermal fluctuations we quite quickly discover that the crystal structure is unstable and the colloids cluster into a denser grouping within the periodic unit cell as seen in Fig. 8. We therefore conclude that the diamond lattice is not even a locally stable state. This is not that surprising given the lack of lattice symmetries seen in the corresponding defect structure in Fig. 1.

We now examine the BCC crystal in the cholesteric with pitch $88\Delta x$ which had the lowest energy of any of the colloidal crystals found in any of the cholesteric systems. Therefore, it may be a potential stable crystal. When we add the thermal noise and allow the particles to move in response we find that in this case the particles fluctuate about the lattice locations. In order to investigate the stability of BCC lattice, the phonon spectrum corresponding to the vibrational modes of the crystal is found by calculating the eigenvalues of the dynamical matrix (the details can be found in Ref. [25]). As the phonon frequencies can be directly related to second derivative with respect to particle location of the effective energy of the crystal, this is equivalent to the second derivative test for a minima familiar from first year calculus. If all the phonon frequencies are real and positive, then the crystal should be locally stable.

In order to accurately find the particles vibrations, we used two BCC unit cells put together. However, there will still be

(a)

(b)

(c)
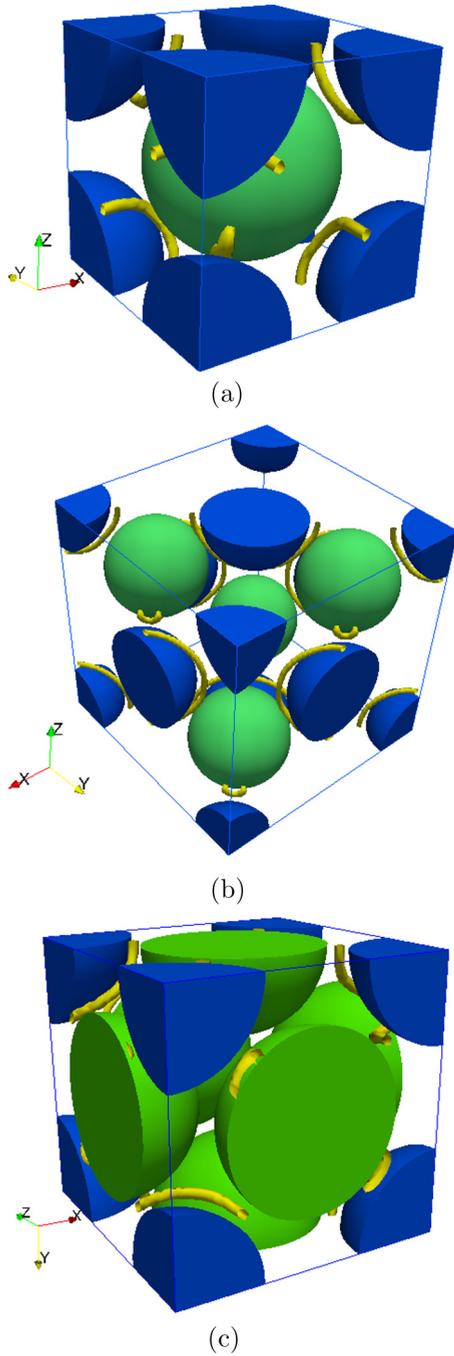
FIG. 7. The lowest energy defect structures found for (a) a BCC colloidal crystal, (b) diamond colloidal crystal, and (c) FCC colloidal crystal inside a nematic LC.

some finite-size effects present in our simulations. Using the minimum energy BCC found before, we added noise to the system and applied LC forces on the colloids to measure the particle displacements and calculate the phonon spectrum. We discarded the first 100 000 time steps to ensure we were following the equilibrium state.

A BCC irreducible Brillouin zone with its reciprocal lattice points is considered in order to map out the crystal phonon frequencies. We chose the path along points Γ, H, N, Γ, P, and H as can be seen in Fig. 9(a) and then calculated the
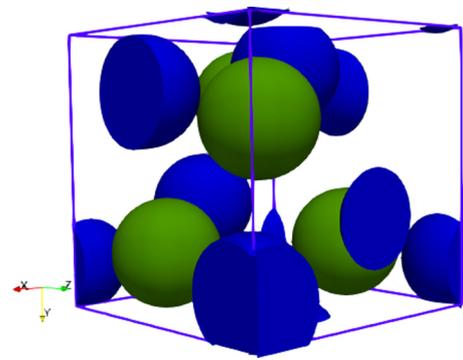
FIG. 8. Displaced colloids that were initially in the lowest energy state found for a diamond lattice [cf. Fig. 1(c)] and then subject to thermal noise.

eigenvalues of the dynamical matrix by using the particles displacements. As shown in Fig. 10(a), all the eigenvalues are positive, which shows there is a local minimum energy corresponding to the second derivative of the potential energy.

(a)

(b)

FIG. 9. Irreducible Brillouin zone for the (a) BCC lattice and (b) FCC lattice.

FIG. 10. Phonon frequencies of (a) BCC lattice in cholesteric and (b) FCC lattice in a nematic. The data were divided into 10 bins, and the error bars corresponds to the standard deviation of the frequencies.

points Γ, X, W, and L on the FCC BZ and calculated the phonon frequencies from simulation data of the fluctuating particles. As can be seen in Fig. 10(b), the eigenvalues of dynamical matrix are all positive showing that the FCC crystal in a nematic LC can be considered as a stable crystal structure.

IV. DISCUSSION AND CONCLUSIONS

In this paper, we examined the energy and stability of a non-closed-packed crystal (diamond) and a closed-packed crystal (BCC) with basis colloids of binary boundary conditions inside a cholesteric LC with a variety of pitch values. Comparing the energy gained by a pair of colloids and different defect structures, we found that the BCC lattice has a high likelihood to be formed in a cholesteric LC. The energy is lower for the BCC crystal inside a cholesteric LC with the pitch value such that the director would be expected to twist by π over one unit cell of the lattice. In investigating the stability of the lattice structures, the diamond crystal in a cholesteric was not found to be stable. The stability of binary BCC lattice was investigated through calculating the phonon frequencies. The positive real frequencies suggests the BCC lattice is stable. We also examined simulations for FCC, BCC, and diamond lattices in a nematic LC, and it can be concluded that the FCC lattice is the most energetically favorable lattice in a nematic LC and is also stable to fluctuations.

It would be interesting to examine how application of an external electric field could influence the stability of the crystal structures found. Such fields change the total LC free energy. Depending on the direction the field is applied, the defects around the particles may be altered as the field affects the orientation of LC molecules. This could also result in different types of induced interactions leading to different interaction energy landscapes. It would also be interesting to examine confined crystals where the defects in the crystal structure could interact with defects on the boundary of the domain.

It is therefore fairly probable that pairs of binary colloids will self-assemble into BCC lattice structure.

Considering crystals in a nematic LC, if we compare the energy per particle for BCC, FCC, and diamond lattices, then we can see that FCC appears to be the most energetically favorable lattice generated in a nematic LC, which is consistent with the results found in [26,27], suggesting that a binary system of colloids in a nematic LC can be arranged into a 2D square lattices or linear chain configurations. Therefore, the stability of the FCC lattice in the nematic is also investigated by adding noise to the system. The Fig. 9(b) shows the first irreducible Brillouin zone (BZ) for FCC lattice. We chose

[1] A. Martinez, H. C. Mireles, and I. I. Smalyukh, Proc. Nat. Acad. Sci. USA **108**, 20891 (2011).

[2] Q. Li, *Liquid Crystals Beyond Displays: Chemistry, Physics, and Applications* (John Wiley & Sons, New York, 2012).

[3] F. Li, J. West, A. Glushchenko, C. I. Cheon, and Y. Reznikov, J. Soc. Inf. Disp. **14**, 523 (2006).

[4] Y. Xia, B. Gates, and Z.-Y. Li, Adv. Mater. **13**, 409 (2001).

[5] M. Skorobogatiy and J. Yang, *Fundamentals of Photonic Crystal Guiding* (Cambridge Unniversity Press, Cambridge, 2009).

[6] J. Ge and Y. Yin, Angew. Chem., Int. Ed. Engl. **50**, 1492 (2011).

[7] J. Joannopoulos, S. Johnson, J. Winn, and R. Meade, *Photonic Crystals: Molding the Flow of Light,* 2nd ed. (Princeton University Press, Princeton, NJ, 2008).

[8] M. Florescu, S. Torquato, and P. J. Steinhardt, Phys. Rev. B **80**, 155112 (2009).

[9] K. M. Ho, C. T. Chan, and C. M. Soukoulis, Phys. Rev. Lett. **65**, 3152 (1990).

[10] S. Changizrezaei and C. Denniston, Phys. Rev. E **96**, 032702 (2017).

[11] P. Poulin and D. A. Weitz, Phys. Rev. E **57**, 626 (1998).

[12] H. Stark, Phys. Rep. **351**, 387 (2001).

[13] F. E. Mackay and C. Denniston, Soft Matter **9**, 5285 (2013).

[14] J. S. Lintuvuori, K. Stratford, M. E. Cates, and D. Marenduzzo, Phys. Rev. Lett. **107**, 267802 (2011).

[15] O. Guzmán, E. B. Kim, S. Grollau, N. L. Abbott, and J. J. de Pablo, Phys. Rev. Lett. **91**, 235507 (2003).

[16] M. R. Mozaffari, M. Babadi, J.-i. Fukuda, and M. R. Ejtehadi, Soft Matter **7**, 1107 (2011).

[17] F. E. Mackay and C. Denniston, Europhys. Lett. **94**, 66003 (2011).

[18] M. Tasinkevych, N. M. Silvestre, and M. M. T. da Gama, New J. Phys. **14**, 073030 (2012).

[19] T. C. Lubensky, D. Pettey, N. Currier, and H. Stark, Phys. Rev. E **57**, 610 (1998).

[20] Y. Gu and N. L. Abbott, Phys. Rev. Lett. **85**, 4719 (2000).

[21] O. V. Kuksenok, R. W. Ruhwandl, S. V. Shiyanovskii, and E. M. Terentjev, Phys. Rev. E **54**, 5198 (1996).

[22] M. Kleman and O. D. Lavrentovich, Philos. Mag. **86**, 4117 (2006).

[23] M. Ravnik, G. P. Alexander, J. M. Yeomans, and S. Zumer, Proc. Nat. Acad. Sci. USA **108**, 5188 (2011).

[24] K. Stratford, O. Henrich, J. S. Lintuvuori, M. E. Cates, and D. Marenduzzo, Nat. Commun. **5**, 3954 (2014).

[25] F. E. Mackay and C. Denniston, Soft Matter **10**, 4430 (2014).

[26] U. M. Ognysta, A. B. Nych, V. A. Uzunova, V. M. Pergamenschik, V. G. Nazarenko, M. Škarabot, and I. Mušević, Phys. Rev. E **83**, 041709 (2011).

[27] S. Changizrezaei and C. Denniston, Phys. Rev. E **95**, 052703 (2017).

[28] P. G. de Gennes and J. Prost, *The Physics of Liquid Crystals* (Oxford University Press, Oxford, 1993).

[29] A. N. Beris and B. J. Edwards, *Thermodynamics of Flowing Systems: With Internal Microstructure*, Oxford Engineering Science Series (Oxford University Press, Oxford, 1994).

[30] J.-B. Fournier and P. Galatola, Europhys. Lett. **72**, 403 (2005).

[31] C. Denniston, D. Marenduzzo, E. Orlandini, and J. Yeomans, Philos. Trans. R. Soc. Lond. A **362**, 1745 (2004).

[32] G. Tóth, C. Denniston, and J. M. Yeomans, Phys. Rev. E **67**, 051705 (2003).

[33] C. Denniston, E. Orlandini, and J. M. Yeomans, Phys. Rev. E **63**, 056702 (2001).

[34] C. Denniston, E. Orlandini, and J. M. Yeomans, Europhys. Lett. **52**, 481 (2000).

[35] C. J. Smith and C. Denniston, J. Appl. Phys. **101**, 014305 (2007).

[36] A. Antipova and C. Denniston, Soft Matter **12**, 1279 (2016).

[37] A. Antipova and C. Denniston, Phys. Rev. E **94**, 052704 (2016).

[38] F. Mackay, S. Ollila, and C. Denniston, Comput. Phys. Commun. **184**, 2021 (2013).

[39] F. Mackay and C. Denniston, J. Comput. Phys. **237**, 289 (2013).

[40] S. Plimpton, J. Comput. Phys. **117**, 1 (1995).

[41] J. S. Lintuvuori, D. Marenduzzo, K. Stratford, and M. E. Cates, J. Mater. Chem. **20**, 10547 (2010).